



# Implementation and evaluation of open boundary conditions for sea ice in a regional coupled ocean (ROMS) and sea ice (CICE) modeling system

Pedro Duarte<sup>1</sup>, Jostein Brændshøi<sup>2</sup>, Dmitry Shcherbin<sup>1</sup>, Pauline Barras<sup>1</sup>, Jon Albretsen<sup>3</sup>, Yvonne Gusdal<sup>2</sup>, Nicholas Szapiro<sup>2</sup>, Andreas Martinsen<sup>1</sup>, Annette Samuelsen<sup>4</sup>, Keguang Wang<sup>2</sup>, and Jens Boldingh Debernard<sup>2</sup>

<sup>1</sup>Norwegian Polar Institute, Fram Centre, Tromsø, Norway

<sup>2</sup>The Norwegian Meteorological Institute, Oslo, Norway

<sup>3</sup>Institute of Marine Research, P.O. Box 1870 Nordnes, 5817 Bergen, Norway

<sup>4</sup>Nansen Environmental and Remote Sensing Centre, Bergen, Norway

**Correspondence:** Pedro Duarte (pedro.duarte@npolar.no)

Received: 26 January 2022 – Discussion started: 8 February 2022

Revised: 13 May 2022 – Accepted: 16 May 2022 – Published: 9 June 2022

**Abstract.** The Los Alamos Sea Ice Model (CICE) is used by several Earth system models where sea ice boundary conditions are not necessary, given their global scope. However, regional and local implementations of sea ice models require boundary conditions describing the time changes of the sea ice and snow being exchanged across the boundaries of the model domain. The physical detail of these boundary conditions regarding, for example, the usage of different sea ice thickness categories or the vertical resolution of thermodynamic properties, must be considered when matching them with the requirements of the sea ice model. Available satellite products do not include all required data. Therefore, the most straightforward way of getting sea ice boundary conditions is from a larger-scale model. The main goal of our study is to describe and evaluate the implementation of time-varying sea ice boundaries in the CICE model using two regional coupled ocean–sea ice models, both covering a large part of the Barents Sea and areas around Svalbard: the Barents-2.5 km, implemented at the Norwegian Meteorological Institute (MET), and the Svalbard 4 km (S4K) model, implemented at the Norwegian Polar Institute (NPI). We use the TOPAZ4 model and a Pan-Arctic 4 km resolution model (A4) to generate the boundary conditions for the sea ice and the ocean. The Barents-2.5 km model is MET's main forecasting model for ocean state and sea ice in the Barents Sea. The S4K model covers a similar domain but it is used mainly for research purposes. Obtained results show significant im-

provements in the performance of the Barents-2.5 km model after the implementation of the time-varying boundary conditions. The performance of the S4K model in terms of sea ice and snow thickness is comparable to that of the TOPAZ4 system but with more accurate results regarding the oceanic component because of using ocean boundary conditions from the A4 model. The implementation of time-varying boundary conditions described in this study is similar regardless of the CICE versions used in different models. The main challenge remains the handling of data from larger models before its usage as boundary conditions for regional/local sea ice models, since mismatches between available model products from the former and specific requirements of the latter are expected, implying case-specific approaches and different assumptions. Ideally, model setups should be as similar as possible to allow a smoother transition from larger to smaller domains.

## 1 Introduction

Global, Arctic or Antarctic wide applications of the Los Alamos Sea Ice Model (CICE) do not require any specific treatment regarding sea ice boundary conditions because the model domain is larger than the areas where sea ice may occur. However, this is not the case of regional implementations of the CICE or any other sea ice models. For such regional

cases, the past and current versions of CICE include a simple way of dealing with open boundaries, restoring them every time step to the initial ice state or to some predefined value, using a relaxation timescale. In the words of Hunke et al. (2015), this implementation is only intended to “provide the hooks” for more sophisticated treatments. Therefore, the main goal of our study is to describe and evaluate the implementation of sea ice time-varying boundaries in the Los Alamos Sea Ice Model using two regional models: the Barents-2.5 km, implemented at the Norwegian Meteorological Institute (MET), and the Svalbard 4 km (S4K) model, implemented at the Norwegian Polar Institute (NPI). We have chosen to use these two models because the former is an operational forecasting system, using data assimilation and used for relatively short-term simulations (a few days); the latter is a research tool used for hindcast and forecast longer-term simulations (a few years), without data assimilation, and this allowed us to evaluate the time-varying boundary scheme for different types of models and simulations.

The use of sea ice models developed for large scales (like CICE) for small-scale forecasts was discussed by Hunke et al. (2020). On the scales of the Barents-2.5 km and S4K models, the use of a continuum hypothesis and the viscous plastic rheology is far from optimal. However, for coupled sea ice–ocean forecasts, good thermal and dynamical forcing and handling of ice–ocean fluxes are also very important for the usefulness and quality of the forecasts. Also, knowledge about the possibility of ice in an area might be more important for applications, such as navigation, than the specific details of the sea ice cover. Therefore, we think adding capability to handle open boundary conditions in the sea ice model can increase the usefulness of small-scale regional coupled model systems for many applications.

Examples of regional implementations of sea ice models may be found in, e.g., Smedsrud et al. (2006), Rousset et al. (2015) and Prakash et al. (2022). Smedsrud et al. (2006) used the Regional Ocean Modeling System (ROMS, <https://www.myroms.org/>, last access: 17 May 2022) to run a high-resolution model of a polynya within a larger domain model. ROMS was used both for the ocean and the sea ice. A relaxation open boundary scheme was used for ocean and ice variables between the nested models. No details are given about the implied technicalities. Prakash et al. (2022) forced sea ice variables in their regional ocean domain and therefore did not need to impose sea ice boundaries of any type. Rousset et al. (2015) describe the implementation of lateral boundary conditions in the Louvain-La-Neuve sea ice model LIM3.6. We are not aware of any comprehensive description of sea ice time-varying boundaries for the CICE model.

## 2 Methods

### 2.1 Model description

We use The Regional Ocean Modeling System (ROMS, <https://www.myroms.org/>, last access: 17 May 2022) and CICE. The software changes described herein are focused on the latter model. The CICE model is managed by the CICE Consortium with an active forum (<https://bb.cgd.ucar.edu/cesm/forums/cice-consortium.146/>, last access: 17 May 2022) and a Git repository <https://github.com/CICE-Consortium>, last access: 17 May 2022). It includes two independent packages: CICE and Icepack. Sea ice dynamics is handled by CICE and sea ice columnar processes (thermodynamics and biogeochemistry) are handled by Icepack. Previous versions did not have such a separation, but the code evolved over the last years towards a clear distinction between processes which are mainly horizontal and those that are mainly vertical/columnar (since CICE6). Various (older) versions of the CICE model are still in use by several modeling systems, including some Earth system models that are part of CMIP6, e.g., CICE 4.1, 5.1 and 5.1.2 (see Roberts et al., 2015; Rasmussen et al., 2018; Wei et al., 2020; and Smith et al., 2021). Scientific and technical details about the Los Alamos Sea Ice Model may be found in Hunke et al. (2015), Jeffery et al. (2016), the forum and the Git repository mentioned above.

#### 2.1.1 Coupling between ROMS and CICE

The coupling between ROMS and CICE was implemented at the Norwegian Meteorological Institute by using the Model Coupling Toolkit (MCT, <https://www.mcs.anl.gov/research/projects/mct/>, last access: 17 May 2022) and creating the METROMS framework mentioned above (e.g., Fritzner et al., 2019, <https://doi.org/10.5281/zenodo.5067164>). An early version of METROMS was also used by Naughten et al. (2017, 2018) and the coupling was very briefly described in those papers. ROMS is the controlling software acting through the CICE drivers CICE\_InitMod.F90, CICE\_RunMod.F90 and CICE\_FinalMod.F90 to initialize, run and finalize CICE (these drivers are called from ROMS master routine – master.F). The variables exchanged through MCT are detailed in Table 1. The underlying philosophy behind the coupling is that fluxes are calculated in the model with most details of the underlying process and then passed conservatively to the other. Thus, all fluxes except the production of “frazil ice” are calculated in the ice model. Frazil ice production is simplified. First, the energy used to increase ocean temperature to the freezing point is calculated in ROMS when forcing has produced under-cooled water. This energy deficit is then passed to the CICE model (frzmlt variable in Table 1) and converted to a suitable amount of consolidated ice with heat and salt content consistent with the

forcing. Any salt expelled from the ice by this process is then passed back again to ROMS.

Exchange frequency between the models depends on synchronization time step and must be a common multiple of involved model time steps. In default setups, the models run concurrently on separate sets of compute cores, with a delayed exchange of fields, such that information calculated in one component is used in the other at the next coupling time interval. The coupled variables are declared in both ROMS and CICE and transferred both ways through MCT routines utilizing the underlying MPI library.

### 2.1.2 Barents-2.5 km model

The Barents-2.5 km model is MET Norway's primary model for forecasting of sea ice conditions in the northern regions. It consists of a fully coupled ocean and sea ice model that covers the Barents Sea and areas around Svalbard (Fig. 1). The modeling system employs the METROMS (<https://doi.org/10.5281/zenodo.5067164>) framework which implements the coupling between the ocean component (Regional Ocean Modeling System, ROMS3.7, <https://www.myroms.org/>, last access: 17 May 2022) and the sea ice component (the Los Alamos Sea Ice Model, CICE5.1.2, <https://www.osti.gov/biblio/1364126-cice-los-alamos-sea-ice-model>, last access: 17 May 2022) (e.g., Fritzner et al., 2019) (for details on coupling, refer to Sect. 2.1.1). The model uses a grid with equally spaced points (2.5 km) in the horizontal and differentially spaced (42 layers) terrain-following vertical coordinates (as the standard ROMS). The ice is distributed among five thickness categories with the lower boundary values of 0.00, 0.64, 1.39, 2.47 and 4.57 m. There are seven vertical layers and one snow layer for each category. Both the ocean and sea ice utilize atmospheric forcing by AROME-Arctic, MET Norway's own numerical weather prediction model for the Arctic (<https://www.met.no/en/projects/The-weather-model-AROME-Arctic>, last access: 17 May 2022; Müller et al., 2017). Considering that this model uses the exact same spatial grid as Barents-2.5 km, our ocean and sea ice experience atmospheric forcing without the loss of accuracy through processes like interpolation. Both ocean and sea ice use boundary conditions from TOPAZ4 (Sakov et al., 2012; Xie et al., 2017), which is a well-tested and documented assimilative (ensemble Kalman filter) coupled ocean and sea ice model covering the Arctic and North Atlantic oceans with operational fields readily available daily. The TPXO7.2 tidal model (Egbert and Erofeeva, 2002) is used for tidal input. The river runoff climatology is based on the Norwegian Water Resources and Energy Directorate (NVE, <http://nve.no>, last access: 17 May 2022) data for mainland Norway (Beldring et al., 2003) and the AHYPE hydrological model for Svalbard and Russia (<https://www.smhi.se/en/research/research-departments/hydrology/hype-our-hydrological-model-1.7994>, last ac-

cess: 17 May 2022). The bathymetry is a smoothed version made from the IBCAO v3 dataset (Jakobsson et al., 2012). Operationally, the model assimilates AMSR2 sea ice concentration from the University of Bremen ([https://seaice.uni-bremen.de/data/amr2/asi\\_daygrid\\_swath/n6250/](https://seaice.uni-bremen.de/data/amr2/asi_daygrid_swath/n6250/), last access: 17 May 2022) over a 24 h analysis run (details on assimilation and downscaling are given below Sect. 2.3.1). Then, using the improved initial condition, a 66 h forecast is produced. The operational archive of the model is located at <https://thredds.met.no/thredds/fou-hi/barents25.html> (last access: 17 May 2022). In this model, ocean boundaries are open, whilst sea ice boundaries were closed, until the implementation of the time-varying boundaries described in this work. The model has been run operationally from March 2019 and its results were evaluated against observations.

### 2.1.3 S4K model

The S4K model has a slightly different domain than the Barents-2.5 km model (Fig. 1) and lower horizontal (4 km) and vertical (35 sigma layers) resolution in the ocean, while the configuration of ice thickness categories and vertical discretization is the same in both setups. The domain covers a slightly different area to allow producing boundary conditions for fjord models in Eastern Greenland. It is based on METROMS coupled with an earlier “columnar” version of CICE, with a “column package” for thermodynamics and biogeochemical processes developed as part of the Accelerated Climate Model for Energy (ACME) project, close to CICE6.0.0 alpha (<https://github.com/CICE-Consortium/CICE/wiki/CICE-Release-Table>, last access: 17 May 2022), following the same procedure described above for the Barents-2.5 km model (<https://doi.org/10.5281/zenodo.5815093>) (see Sect. 2.1.2). The ocean and sea ice are forced with atmospheric fields from ECMWF reanalysis v5 (ERA5, <https://www.ecmwf.int/en/forecasts/dataset/ecmwf-reanalysis-v5>, last access: 17 May 2022). River forcing is based on ArcticRims (<https://rims.unh.edu>, last access: 17 May 2022) for Russia and North America, catchment area discharge estimates from the NVE (<http://nve.no>, last access: 17 May 2022) for northern Norway, and Mernild and Liston (2012) for Greenland. Sea ice boundary conditions are from TOPAZ4 (Sakov et al., 2012; Xie et al., 2017) and ocean boundary conditions are from the Pan-Arctic 4 km resolution model (A4) model (Hattermann et al., 2016). This model was run continuously from August 2014 until July 2015 and its results evaluated against observations detailed in Sect. 2.3.2.

**Table 1.** Data exchange between ROMS and CICE through MCT (see text).

| From ROMS to CICE                             |                   | From CICE to ROMS   |                    |
|---|-------------------|---|--------------------|
| Name and abbreviation                         | Dimensions        | Name and abbreviation   | Dimensions         |
| Sea surface salinity (sss)                    | psu               | Ice concentration (aice)  | dimensionless      |
| Sea surface temperature (sst)                 | °C                | Freshwater flux from ice (freshAI)  | kg s <sup>-1</sup> |
| Melt-freeze potential (frzmlt)                | W m <sup>-2</sup> | Salt flux from ice (fsaltAI)  | kg s <sup>-1</sup> |
| Velocity components ( <i>u</i> and <i>v</i> ) | m s <sup>-1</sup> | Non-radiative heat flux from ice (fhocnAI)                                  | W m <sup>-2</sup>  |
| Free surface height (ssh)                     | m                 | Radiative heat flux through sea ice (fswthruAI)                             | W m <sup>-2</sup>  |
|   |                   | Stress components in <i>x</i> and <i>y</i> directions (strocnx and strocny) | N m <sup>-2</sup>  |

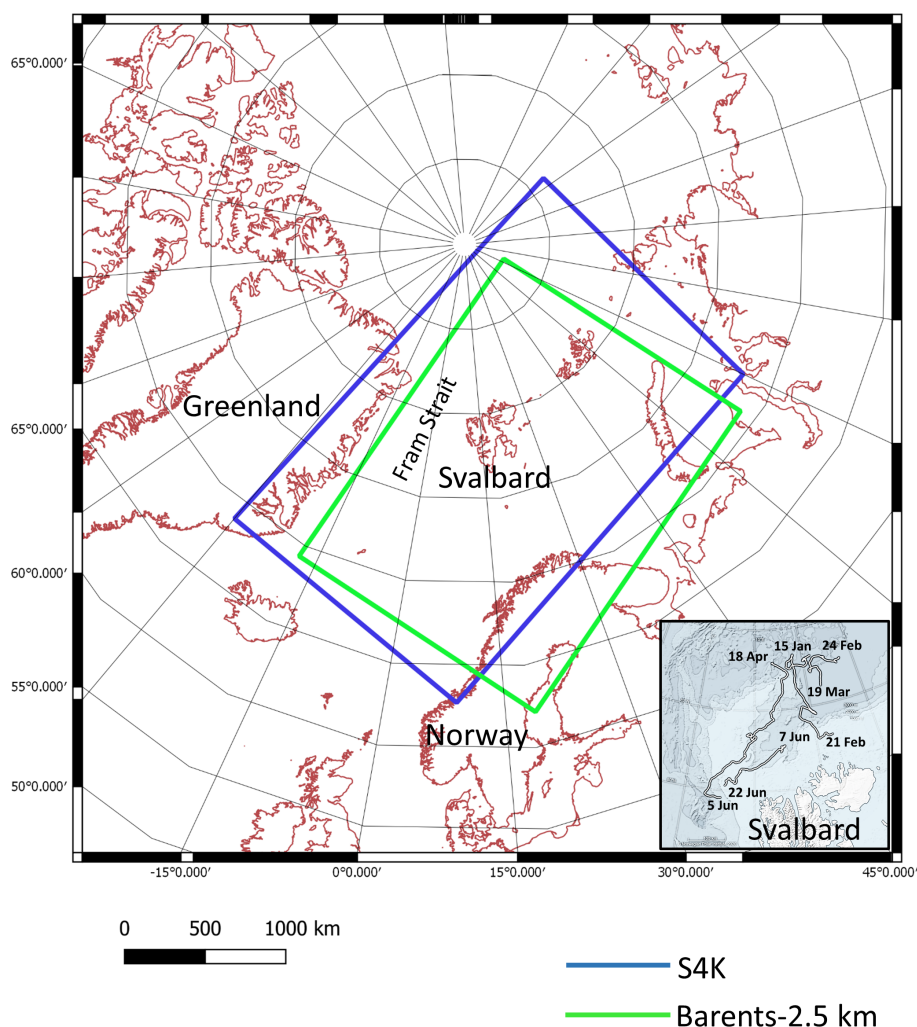


**Figure 1.** Barents-2.5 km and S4K model domains. The insert in the bottom right corner represents Svalbard and the area where the various drifts (lines showing the start and end dates of each drift) of the N-ICE2015 expedition (Granskog et al., 2018) took place and along which sea ice and ocean data detailed in Table 5 were collected.

## 2.2 Implementation of time-varying boundary condition in the Los Alamos Sea Ice Model

### 2.2.1 Software details

We describe the main code changes in Table 2. We defined a Boolean variable (`sea_ice_time_bry`) that must be set to *True* in the CICE input file (`ice_in`) whenever time-dependent boundary fields are used. The main CICE model drivers (`CICE_InitMod.F90` and `CICE_RunMod.F90`) were modified. The first one initializes and the second runs the model. The initialization driver now includes a call to a routine located in the file containing CICE forcing routines (`ice_forcing.F90`) that initializes boundary variables when `sea_ice_time_bry = True`. Similarly, the run driver includes a call to a subroutine in `ice_forcing.F90` that updates the boundary variables at each time step. Updating implies reading boundary fields from boundary files and interpolating them to the model time step. Details on the boundary files are given below.

The new boundary variables match CICE variables. They have a prefix corresponding to the name of the corresponding variable in CICE (Table 2) followed by an underscore and the suffix “bry”. We separated the new variables into ice-category-dependent two- and three-dimensional (2-D and 3-D) and ice-category-independent variables (Table 2). The 2-D variables represent either surface sea ice properties or bulk properties of ice or snow. The 3-D variables represent properties that vary vertically in the ice or snow and are resolved as a function of the number of ice and snow layers defined for a simulation. The ice-category-dependent variables have a dimension used to store the values of different ice thickness categories, defined as a function of sea ice thickness. For details on CICE size thickness categories, see Hunke et al. (2015).

We allocate to the boundary variables the same dimensions allocated for the matching CICE variables, even though we need to track their values only along the open boundaries. This occupies more memory than necessary, with boundary variable “working” rectangular arrays being filled with zeros except for the boundary cells, but it simplifies the process of scattering variable values among different tiles in a parallel run, since we may reuse CICE data scattering routines. However, as described below, the boundary NetCDF files have only vector arrays and do not require “extra” space as the working arrays (see below).

The CICE file with more modifications for the time-varying boundary implementation is `ice_forcing.F90` (Table 2). New routines were created to construct boundary file names, to read these files and to make the necessary time interpolations. Some specific file reading routines were implemented in `ice_read_write.F90` given the format of boundary files (see below). These routines are called from `ice_forcing.F90`.

Boundary restoring takes place in file `ice_restoring.F90`, where the boundary values updated in `ice_forcing.F90` are used to modify the corresponding CICE variables using a relaxation time defined in `ice_in` (`trestore`), along the “halo” cells (Hunke et al., 2015) located at the northern, southern, western and eastern limits of the model domain and their neighbor cells within the domain. These updates occur in the routine `ice_HaloRestore` that was modified from its original version. Snow and ice enthalpies are calculated from corresponding temperatures. In the tests carried out so far, we “relaxed” only the cells detailed above to follow exactly the way CICE deals with boundary conditions but a more complex treatment involving a larger relaxation zone may be considered.

Minor adjustments were implemented for Barents-2.5 km to enhance reliability for the operational system, particularly to blend mismatches between the external and internal solutions. In `ice_HaloRestore`, the first physical points as well as the halos are restored/nudged. Dynamical variables `uvel`, `vvel`, `divu`, shear and strength are restored to the neighboring interior point. Several technical additions address edge cases. Additional grid variables are extrapolated to halo cells (`ice_grid.F90`). Halo cells are no longer zeroed during multiprocessor communications (`ice_boundary.F90`). Boundary values are restored before both thermodynamics and dynamics (in `CICE_RunMod.F90`), which is necessary for prescribing boundary values (i.e., when `trestore = 0`).

In the S4K model, the only exception in the boundary restoring process is with `uvel` and `vvel`, which are restored as any other boundary variable when there is sea ice outside the domain, else internal velocities are assumed in line with Rousset et al. (2015). This is to guarantee that the sea ice motion inside the model domain is properly affected by larger-scale drift trends in “long-term” simulations (several months).

Our approach differs from that described by Rousset et al. (2015) for the lateral boundary conditions in the Louvain-La-Neuve sea ice model (LIM3.6) in that we restore tracer boundary values irrespective of the velocity direction across the boundaries. Moreover, we do not fill the boundaries with ice thickness categories following a statistical law – categories are filled depending on their availability in the boundary data. In any case, specific changes can be easily made in the code to test different settings.

### 2.2.2 Boundary data details

The main challenge with the boundary data is the matching between available model output for a larger domain and the data needs of CICE. In the examples provided here, we used data from TOPAZ4 as explained above. The available outputs relevant for CICE boundaries include daily values for ice concentration, ice and snow thickness, and ice east–west and south–north velocities. There are no data for ice or snow internal or surface temperatures, or for ice salinity. There are

**Table 2.** Summary of main changes in the Los Alamos Sea Ice Model related to the implementation of time-varying boundaries (<https://doi.org/10.5281/zenodo.5067164> and <https://doi.org/10.5281/zenodo.5815093>) (see text).

| Modified files     | Main changes   |
|--------------------|--|
| ice_in             | The Boolean sea_ice_time_bry was added to the domain name list. Time-varying boundary code is used when this variable is set to true.  |
| CICE_InitMod.F90   | A call to init_forcing_bry – a new subroutine implemented in ice_forcing.F90 (see below) used to initialize the boundaries if the Boolean sea_ice_time_bry is set to true in the model input file (ice_in, see below).   |
| CICE_RunMod.F90    | A call to get_forcing_bry – a new subroutine implemented in ice_forcing.F90 (see below) used to update the boundaries from files if the Boolean sea_ice_time_bry is set to true in the module input file (ice_in).   |
| ice_forcing.F90    | <p>New variables were defined to store boundary values. These parallel all-model variables were updated by the Los Alamos Sea Ice Model in ice_restoring.F90.</p> <p>Ice-category-dependent horizontal (2-D) variables:<br/>aicen_bry [ice concentration], vicen_bry [ice volume per unit area (m)], vsnon_bry [snow volume per unit area (m)], alvln_bry (concentration of level ice), vlvl_n_bry [volume per unit of area of level ice (m)], apondn_bry (melt pond fraction), hpondn_bry [melt pond depth (m)], ipondn_bry [mean pond ice thickness (m)], Tsfc_bry [ice/snow surface temperature (°C)].</p> <p>Ice-category-dependent and vertically resolved (3-D) variables:<br/>Tinz_bry [sea ice inner temperature (°C)], Sinz_bry (sea ice inner bulk salinity) and Tsnz_bry [snow inner temperature (°C)].</p> <p>Ice-category independent horizontal (2-D) variables:<br/>uvel_bry and vvel_bry; <math>x</math> (north/south) and <math>y</math> (west/east) velocity components (<math>\text{m s}^{-1}</math>).</p> <p>New routines were created:<br/>init_forcing_bry – calculates current year and final year in forcing cycle.<br/>boundary_files (and file_year_bry) – constructs boundary file names from current simulated year.<br/>get_forcing_bry – calls boundary_data.<br/>boundary_data – defines working arrays for boundary variables, call routines to read boundary files and to interpolate variable values to the model time step.<br/>read_bry_ice_data_nc interface procedures: read_bry_ice_data_nc_2D, read_bry_ice_data_nc_3D and read_bry_ice_data_nc_4D, to read boundary values from NetCDF files, according to their dimensions calling ice_read_write.F90 routines (see next table line).<br/>interpolate_interpolate_data_n_layer – interpolate boundary data between two consecutive time steps. The former and the latter are used for ice-category-dependent 2-D and 3-D variables, respectively. Other variables reuse the “standard” interpolation routine (interpolate_data).</p> |
| ice_read_write.F90 | Three routines (ice_read_nc_bry_2D, ice_read_nc_bry_3D and ice_read_nc_bry_4D) were added to the interface ice_read_nc to read the different types of boundary data (see above).   |
| ice_restoring.F90  | ice_HaloRestore – this is where boundary values are restored, using boundary data and a user-defined relaxation timescale (trestore) defined in the model input file (ice_in).   |

no data of any kind of ice thickness categories. Therefore, we had to make some assumptions. These will have to be defined for each application depending on available boundary data. In our case, we proceeded as follows:

1. TOPAZ values located along the boundaries of our domains were linearly interpolated to our grids.
2. Ice-category-dependent variables were stored in boundary files assuming the same number of categories used in our runs (five). For each grid point, all values were set to zero, except for the category where available “bulk” ice thickness belonged.
3. Surface (skin) snow or ice temperatures (in the absence of snow) were set to air temperatures taken from the atmospheric forcing files, when air temperature was  $<0$ , else they were set to a slightly negative value ( $-0.00001$  °C).
4. Inner snow and ice temperatures were obtained by linearly interpolating between the surface temperature and the freezing water temperature. The same temperature trend was assumed for snow and ice. Therefore, when snow was present, its height was taken into account as the thickness of each ice layer.

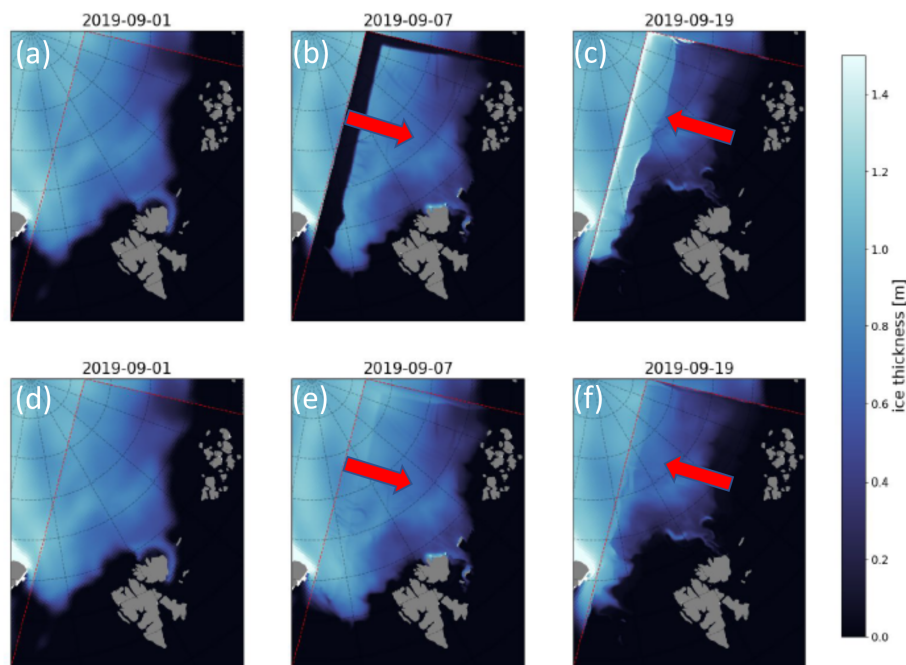


**Figure 2.** Wind-idealized experiments with the Barents-2.5 km model plotted inside the TOPAZ4 model. The Barents-2.5 km model was run in its full state except the wind forcing was idealized in the sense of constant wind in the model  $x_i$  direction. The figure shows sea ice thickness fields at three moments in time for the run without (a–c) and with (d–f) time-varying boundaries. The first column is the initial TOPAZ4 field interpolated onto the Barents-2.5 km grid, the second column corresponds to Barents-2.5 km results after 6 d as the wind turns back in the negative direction, i.e., when the sea ice should be at its maximum displacement relative to the left-most boundary, and the final column shows the state towards the very end of the run when the wind has been blowing “left” for 12 d. Wind direction is shown by the red arrows.

- Inner ice salinities were calculated to match multiyear and first-year ice (MYI and FYI, respectively) profiles described in the literature (Gerland et al., 1999). We assumed that when ice thickness was  $>1.5$  m it was MYI, else it was FYI. In the case of MYI, we used the profiles described in older versions of CICE (Hunke et al., 2015, Eq. 76). In the case of FYI, we assumed a “C”-shaped profile defined by Eq. (1) (e.g., Fig. 3 of Gerland et al., 1999):

$$S_i = 19.539Z_i^2 - 19.93Z_i + 8.913, \quad (1)$$

where  $S_i$  is the salinity and  $Z_i$  is the fractional depth of layer  $i$  – zero at the ice top and 1 at the ice bottom.

Examples of boundary files may be found at <https://doi.org/10.5281/zenodo.5798076>.

## 2.3 Data used for model evaluation

### 2.3.1 Barents-2.5 km model

The data used to evaluate the Barents-2.5 km model can be found in Table 3. For this model system, the focus was purely on remote sensing of sea ice concentration. AMSR2 (<https://seaice.uni-bremen.de/sea-ice-concentration/amsre-amsr2/>,

last access: 17 May 2022) is a passive microwave product with a spatial resolution of 6.25 km (Spreen et al., 2008), consisting of continuous sea ice concentration (SIC) values between 0 and 1.0 (same as the model). The Norwegian ice charts (Dinessen and Hackett, 2016) have a gridding resolution of 1 km and are produced manually based on multiple data sources, where the primary source is radar data (SAR). Since the ice charts consist of discrete values, the modeled SIC is categorized as shown in Table 4. For AMSR2, continuous values are applied. The satellite products are interpolated to the model resolution of 2.5 km, using bi-linear interpolation for the ice charts and the nearest neighbor method (same product as used for assimilation) for the AMSR2 products. In the comparison, all SIC values  $>0$  are included, where land, missing values and open water (in both observations and model) are masked out. This means that the entire sea-ice-covered area inside the domain of the model is included in the comparison. The AMSR2 products are available daily, whereas the Norwegian ice charts are only available during working days.

The data assimilation applied in the operational Barents-2.5 km model is the combined optimal interpolation and nudging (COIN; Wang et al., 2013). It was originally developed for assimilating sea ice concentration in a two-level sea ice model within ROMS and is now fur-

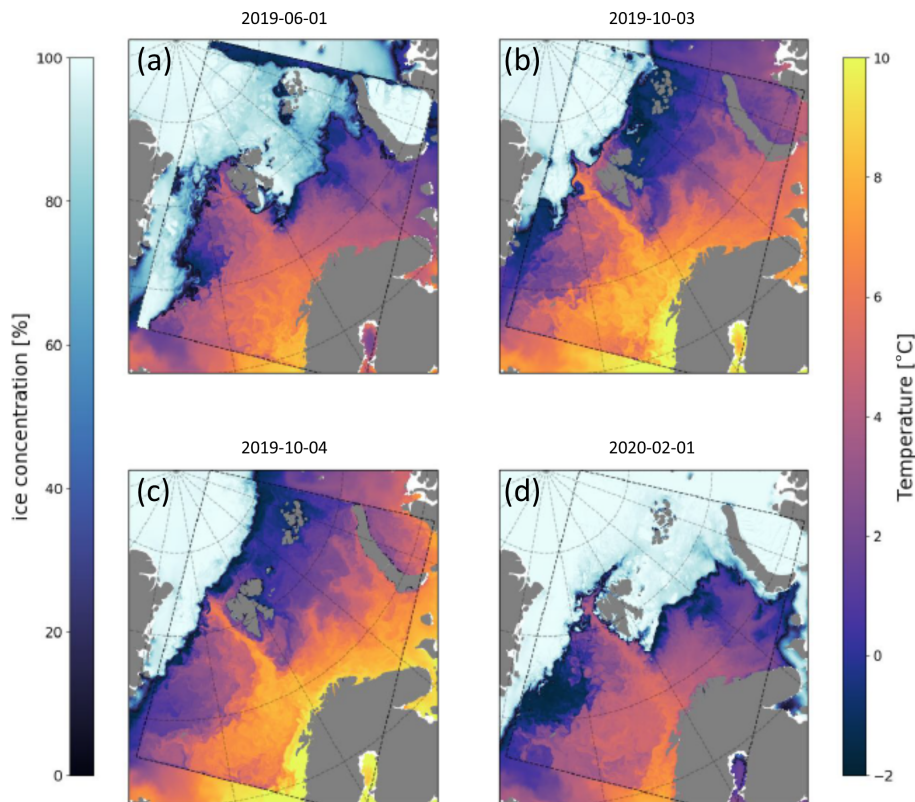


**Figure 3.** Operational simulations with the Barents-2.5 km model, plotted inside the TOPAZ4 model. These plots are taken directly from the operational model at MET and illustrate the effects of time-varying boundary conditions in the operational model. Sea ice concentration and surface water temperature fields (in the open water areas) are shown for three different dates at 00:00 UTC. Panel (a) are a few months before new BCs, (b) the day before new BCs, (c) the day of new BCs and (d) a few months after new BCs.

ther developed for the multi-category CICE model in METROMS (<https://doi.org/10.5281/zenodo.5067164>). The COIN method is a nudging method applied inside the CICE code. The modeled sea ice concentration is updated every model (CICE) time step with a small innovation (difference between model results and observations) such that the final analysis will reach the optimal estimate, which is a linear combination of the model results and the observations based on their variances (Wang et al., 2013). The daily AMSR2 sea ice concentration is assimilated, where the observations standard deviation is calculated according to Spreen et al. (2008), and the model standard deviation is approximated as the absolute difference between the model results and observations following Wang et al. (2013). During the assimilation, the real thickness of each category of snow and sea ice remains unchanged, so their volumes are updated according to the change of the ice concentrations.

### 2.3.2 S4K model

Datasets used for model evaluation are listed in Table 5, with links or citations to the various data sources. These include ocean, sea ice and snow data. We used satellite prod-

ucts and in situ data collected during the N-ICE2015 expedition (Granskog et al., 2018 and Fig. 1). Therefore, more detailed comparisons between observations and model results are given for 2015. We also compare TOPAZ4 reanalysis (<https://doi.org/10.48670/moi-00007>) with S4K model outputs regarding ocean and sea ice variables listed below and in Table 5. Ocean data are used here to evaluate the “context” for the sea ice simulations. It includes vertical profiles obtained with a CTD and with a microstructure profiler during the N-ICE2015 expedition (Table 5).

We used satellite data of sea ice concentrations from regional high-resolution sea ice charts for the Svalbard region (the same mentioned above for the Barents-2.5 km model) and for sea ice and snow thickness from the European radar altimeter CryoSat-2, generated at the Alfred Wegener Institute (AWI) for the winter period (October–April) (Hendricks and Ricker, 2020). We also used CryoSat2-SMOS weekly Arctic sea ice thickness data (Ricker et al., 2017, <https://spaces.awi.de/display/CS2SMOS>, last access: 17 May 2022).

Sea ice plus snow thickness were collected during the N-ICE2015 expedition with a helicopter-borne electromagnetic induction sounding (HEM) (King et al., 2016) and a

**Table 3.** Datasets used for Barents-2.5 km model evaluation. The listed references include links to the repositories where data and details on sampling and data processing can be found.

| Compartment | Variable                          | Description  | References  |
|-------------|-----------------------------------|--|---|
| Sea ice     | Ice concentration (dimensionless) | Regional high-resolution sea ice chart for the Svalbard region | Dinessen and Hackett (2016)<br><a href="https://thredds.met.no/thredds/catalog/myocean/siw-tac/siw-metno-svalbard/catalog.html">https://thredds.met.no/thredds/catalog/myocean/siw-tac/siw-metno-svalbard/catalog.html</a> (last access: 17 May 2022) |
|             |                                   | AMSR2 sea ice concentration product from University of Bremen  | Spren et al. (2008)<br><a href="https://seaice.uni-bremen.de/data/amsr2/asi_daygrid_swath/n6250/">https://seaice.uni-bremen.de/data/amsr2/asi_daygrid_swath/n6250/</a> (last access: 17 May 2022)   |

**Table 4.** Ice concentration values and their categorization used for the ice charts and Barents-2.5 km model validation.

| Ice concentration values | Re-mapped values |
|--------------------------|------------------|
| <0.01                    | 0                |
| 0.01–0.1                 | 0.05             |
| 0.1–0.4                  | 0.25             |
| 0.4–0.7                  | 0.55             |
| 0.7–0.9                  | 0.80             |
| >0.9                     | 0.95             |

ground-based electromagnetic instrument (EM31) (Rösel et al., 2016a) with footprints of approximately 50 and 3–5 m, respectively (Haas et al., 2009). Snow thickness was measured with a Magnaprobe with a footprint of approximately 0.2 m (Rösel, 2016b).

## 2.4 Model simulations

Simulations carried out with the Barents-2.5 km model are short term, in accordance with its operational nature. Model evaluation was based on idealized simulations and on operational simulations and focused on sea ice concentration, which is the main variable of interest for this model. In the case of the S4K model, ~1-year simulations were carried out and comparisons between model and observations were focused on sea ice concentration, ice and snow thickness. Moreover, comparisons for the oceanic variables were also carried out.

### 2.4.1 Barents-2.5 km model

Model experiments with idealized wind forcing have been conducted with the Barents-2.5 km model in order to visually showcase the effects of using time-varying boundary conditions. The model was initialized from TOPAZ4 fields at 1 September 2019 and it ran until 20 September 2019. One run without the time-varying boundaries (just like the operational model ran before) and one with the boundaries ex-

tracted from TOPAZ4 results for the same period. All aspects of the model run, except the wind forcing, were realistic. The wind forcing was idealized to be purely in the model  $xi$  direction, positive in the first part of the run and negative in the latter part of the run. The goal was to blow the sea ice away from the left-most boundary before reversing the wind and observe the interaction with the boundary when the sea ice is forced towards it again. More specifically, the wind forcing was

$$U_{\text{wind}} = \begin{cases} 10.0 \text{ ms}^{-1}, & t \leq 7 \text{ September 2019} \\ -10.0 \text{ ms}^{-1}, & t > 7 \text{ September 2019.} \end{cases}$$

We also compare results obtained with operational simulations before and after the time-varying boundaries were introduced. These contrasting results are also evaluated against the satellite data. The operational model is initialized with data from TOPAZ4. We began using time-varying boundary conditions in the operational forecasts in October 2019 after spinning up the model for 1 month.

### 2.4.2 S4K model

The model was initialized from TOPAZ4 fields and ran from January 2014 until July 2015. Results were analyzed only from October 2014 after some spin-up time. Model output was compared with observations of ocean and sea ice variables measured in situ during the N-ICE2015 expedition (Granskog et al., 2018). Here, we focus only on the evaluation of hydrographical properties with depth and on temperature–salinity diagrams. The satellite data were used mainly for evaluation of sea ice concentration and sea ice and snow thickness (Table 5). Comparisons were also made with TOPAZ4 results since it is an operational system in use by the Copernicus Marine Service (<https://marine.copernicus.eu/>, last access: 17 May 2022) and it provides S4K sea ice boundary conditions. Ocean boundary conditions were from the Pan-Arctic A4 model described in Hattermann et al. (2016). The decision of using ocean boundary conditions from one model and sea ice boundary conditions from another one was based on results from preliminary simulations using only TOPAZ4 ocean and sea ice boundaries. The results of these

**Table 5.** Datasets used for S4K model evaluation. The listed references include links to the repositories where data and details on sampling and data processing can be found. CTD – conductivity–temperature–depth; MSS90L – ocean microstructure profiler; HEM – helicopter-borne electromagnetic induction sounding; EM31 – ground-based electromagnetic instrument.

| Compartment | Variable   | Description   | References   |
|-------------|--|---|--|
| Ocean       | Practical salinity (psu); in situ temperature (°C) | N-ICE2015 ship-based CTD and ocean microstructure profiles (MSS90L)                             | Dodd et al. (2016) and Meyer et al. (2016) for CTD and MSS90L data, respectively           |
| Sea ice     | Ice concentration (dimensionless)                  | Regional high-resolution sea ice charts for the Svalbard region                                 | Dinessen and Hackett (2016)  |
|             | Ice and snow thickness (m)                         | Arctic sea ice freeboard and thickness from the European radar altimeter CryoSat-2              | Hendricks and Ricker (2020)  |
|             |  | CryoSat2-SMOS weekly Arctic sea ice thickness data  | Ricker et al. (2017)   |
|             |  | HEM, EM31 and Magnaprobe data collected during the N-ICE2015 expedition (Granskog et al., 2018) | King et al. (2016) for HEM, Rösel (2016a and b) for EM31 and Magnaprobe data, respectively |

simulations produced an unrealistically weak West Spitsbergen Current and large salinity and temperature ocean biases (not shown). Therefore, we tried using ocean boundaries from the A4 model which led to a significant improvement in our results.

### 3 Results

#### 3.1 Barents-2.5 km model

##### 3.1.1 Idealized simulations

The idealized simulations (results available at <https://zenodo.org/record/4727865#.YOMasRHis2w>, last access: 17 May 2022) show that when time-varying boundaries are not considered, and the wind direction is perpendicular to one of the boundaries, a gap is created between the ice edge of the Barents-2.5 km domain and the boundary with the TOPAZ4 domain (Fig. 2a and b). Moreover, when the wind is reversed, ice piles up at the boundary where the gap was formed, artificially increasing sea ice thickness. These “non-realistic” behaviors disappear once time-varying boundaries are considered, resulting in a relatively smooth transition between the results of TOPAZ4 and those of the Barents-2.5 km model (Fig. 2). This transition is not perfect, and signs of a “seam” can be seen where the external fields have been propagating through the boundary.

##### 3.1.2 Operational simulations

Results from these simulations are available at <https://zenodo.org/record/4728069#.YOMLdHis2w> (last access: 17 May 2022). The upper left panel of Fig. 3 shows typical modeled sea ice concentration fields prior to the usage of time-varying boundary conditions. While the overall field has a lot of details in each panel, there are significant artifacts, especially, along the top boundary. Northeastern winds force ice away from the boundary, leaving open water behind (Fig. 3a), creating an artificial polynya in the Barents-2.5 km. This was a regular occurrence in the original operational model. Figure 3b shows the day before time-varying boundaries (OBCs) were enabled. The more realistic ice field here resulted from re-initializing the model on 3 September 2019 with the TOPAZ4 fields after results shown in Fig. 3a and prior to results shown in Fig. 3b. This was done because the model had severely diverged from the observations. Figure 3c shows the day the OBC fields were put into operation. This represents the 1-month spun-up fields from TOPAZ4, while using time-varying boundary conditions, and immediately exhibits better correspondence with the external fields. Note that, at this point, this is a combined effect of the proximity (in time) to the re-initialization from TOPAZ4 and the effects of the new OBCs. That is why there is such a significant difference over only 1 d. It would have been a lot smaller had the OBCs been put into operation without a spin-up run. Finally, Fig. 3d shows the situation after 4 months of running with the time-varying boundaries (before AMSR2 assimilation was put into operation). We observe a much better agreement between ice fields of TOPAZ4 and those of Barents-2.5 km models.

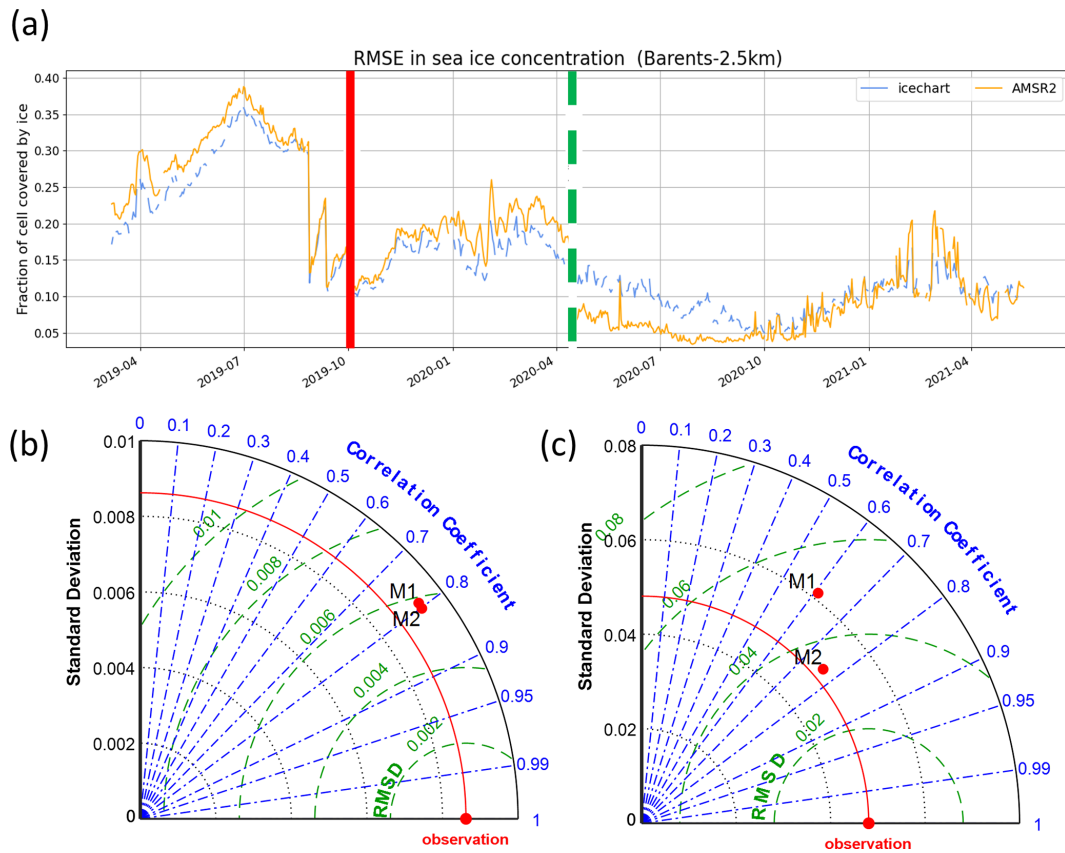


**Figure 4.** (a) Root mean square error (RMSE) of the Barents-2.5 km model for sea ice concentration, before and after using time-varying boundaries (vertical red line) and before and after data assimilation began (dashed vertical green line), calculated against AMRS2 and Svalbard ice chart observations (see Sect. 2.3.1). (b, c) Taylor diagrams for the operational Barents-2.5 km simulations and AMRS2 observations, without (M1) and with (M2) the time-varying boundaries; (b) daily results averaged over the whole model domain; (c) spatially resolved daily results. The red line in the Taylor charts depicts the standard deviation of the observations. The green curved isolines show the RMSE, and the correlation coefficient is shown in blue.

Figure 4a shows the root mean square error (RMSE) of the predicted sea ice concentration from March 2019 to April 2021 in the operational Barents-2.5 km model calculated against AMRS2 and Svalbard ice chart observations, which tracked the performance of the operational Barents-2.5 km in the early 2 years. The vertical red line indicates the time when applying the time-varying boundaries, and the vertical green line shows the time when applying the data assimilation (see Sect. 2.3.1). Before the time-varying boundaries, the RMSE was generally between 0.2 and 0.4 (before mid-August 2019). Due to the large error in the open boundaries, the initial conditions had to be re-initialized in late August and September, which is seen in the abrupt decrease of the RMSE. However, the RMSE increased rapidly after each re-initialization. After implementing the time-varying boundaries in October 2019, the average RMSE is generally below 0.25, much lower than in the previous period. To further analyze the effect of the time-varying boundaries, we computed Taylor diagrams (Taylor, 2001), using the MATLAB PeterRochford-SkillMetricsToolbox-d7ea0d3. The im-

provement in model performance was negligible when the daily total sea ice extent was considered (Fig. 4b). However, a large improvement is apparent when spatially resolved data are compared (Fig. 4c), with higher correlation coefficient and lower RMSE for the simulation with time-varying boundaries. Moreover, the model standard deviation becomes very close to that of the data. Altogether, this shows that the model accuracy improved and that ice concentration variability is better captured.

### 3.2 S4K model

We present first results for ocean variables and then for sea ice variables. In both cases, we compare S4K with TOPAZ4 results and with observations (see Sect. 2.3.2).

#### 3.2.1 Ocean results

Extreme median salinity and temperature biases are  $\sim -0.3$  and  $-4^\circ\text{C}$  and,  $\sim +0.2$  and  $-1.5^\circ\text{C}$ , for TOPAZ4 and S4K, respectively (Figs. 5 and 6). The salinity biases within the

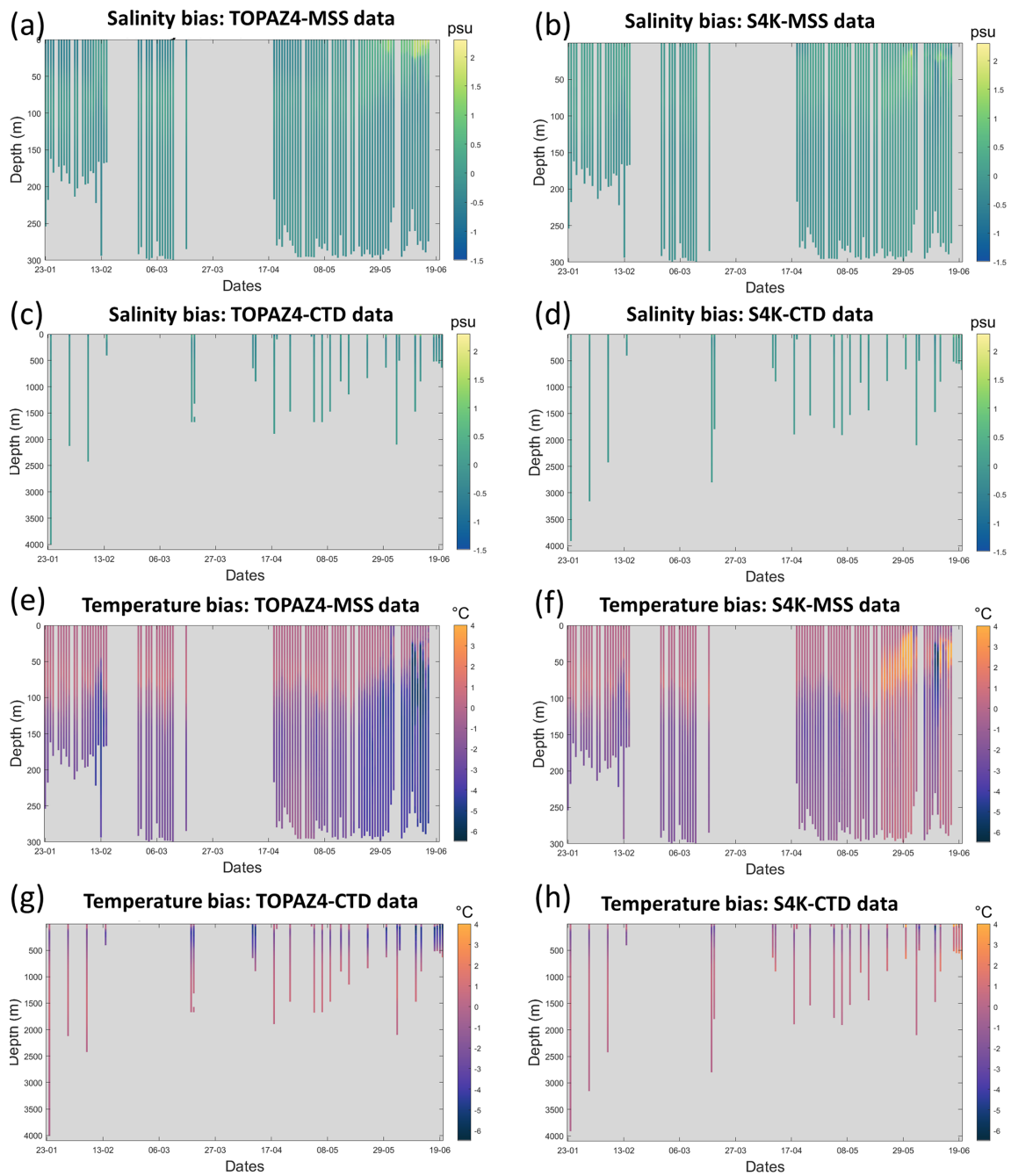


**Figure 5.** TOPAZ4 (a, c, e, g) and S4K (b, d, f, h) model salinity (upper four panels) and temperature (lower four panels) biases, as a function of time and depth, from profiles obtained during the N-ICE2015 expedition (Granskog et al., 2018). Panels (a), (b), (e) and (f) show biases for the upper 300 m, based on data from ocean microstructure profiles (MSS) (Meyer et al., 2016). Panels (c), (d), (g) and (h) show biases for the whole water column, based on CTD profiles (Dodd et al., 2016) (see Fig. 1, Table 5 and text).

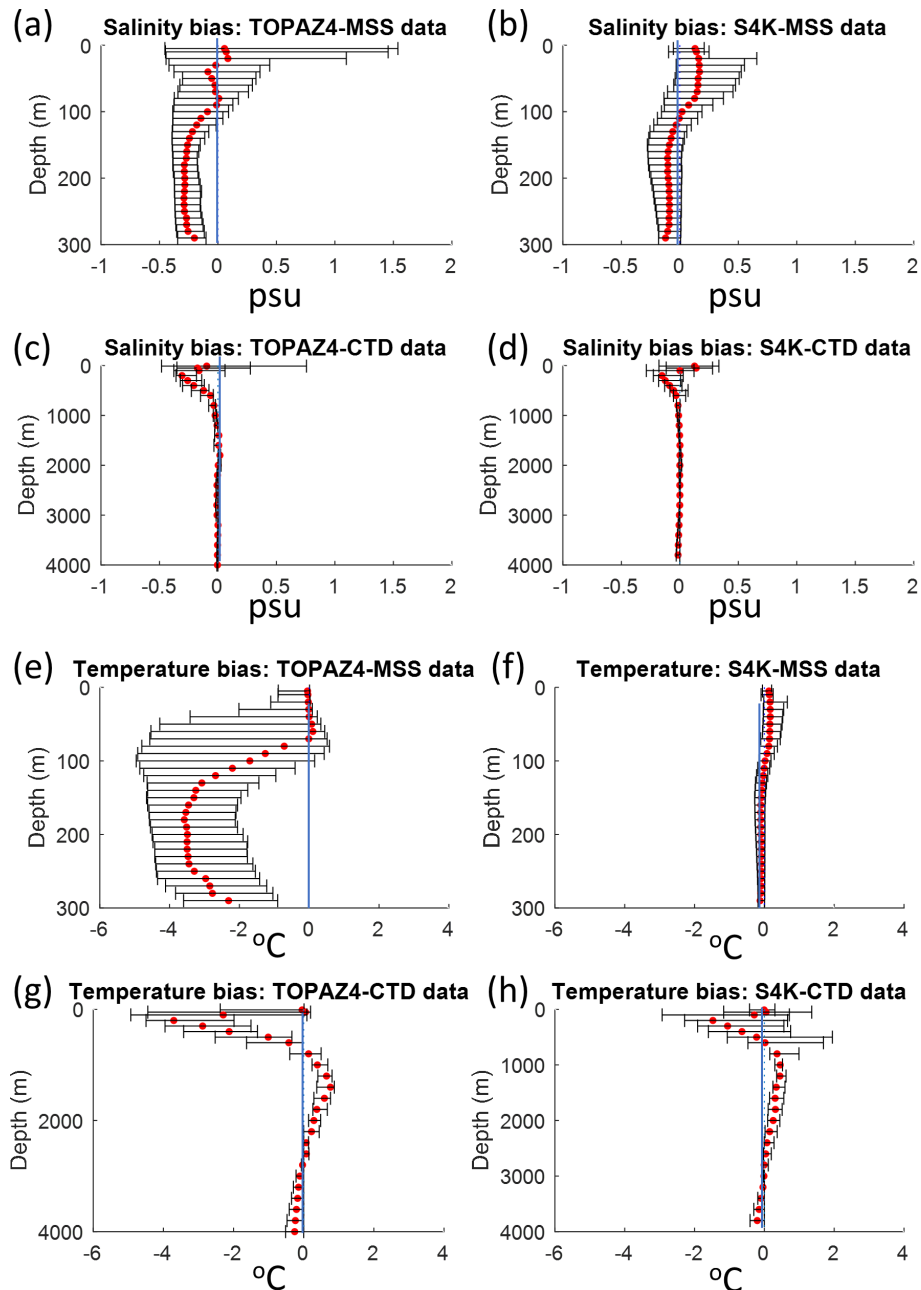


**Figure 6.** Salinity and temperature median bias  $\pm 10$  and 90 percentiles for TOPAZ4 (a, c, e, g) and S4K (b, d, f, h), as a function of depth, based on data obtained during the N-ICE2015 expedition (Granskog et al., 2018). Panels (a), (b), (e) and (f) show biases for the upper 300 m, based on data from ocean microstructure profiles (MSS) (Meyer et al., 2016). Panels (c), (d), (g) and (h) show biases for the whole water column, based on CTD profiles (Dodd et al., 2016) (see Fig. 1, Table 5 and text).

top 100 m are smaller for TOPAZ and less than  $+0.2^{\circ}\text{C}$  for S4K. The temperature biases within the same depth range are smaller for S4K. Both model biases for salinity and temperature are larger between approximately 100 and 300 m than for the other depth ranges (Figs. 5 and 6), being smaller for S4K than for TOPAZ. Temperature–salinity diagrams show better similarity between S4K and observations than between TOPAZ4 and observations (Fig. 7). Salinity and temperature

ranges from S4K compare well with those of the observations (Fig. 7a versus Fig. 7b). In the case of TOPAZ, both ranges are much narrower than those of the observations (Fig. 7a versus Fig. 7b).

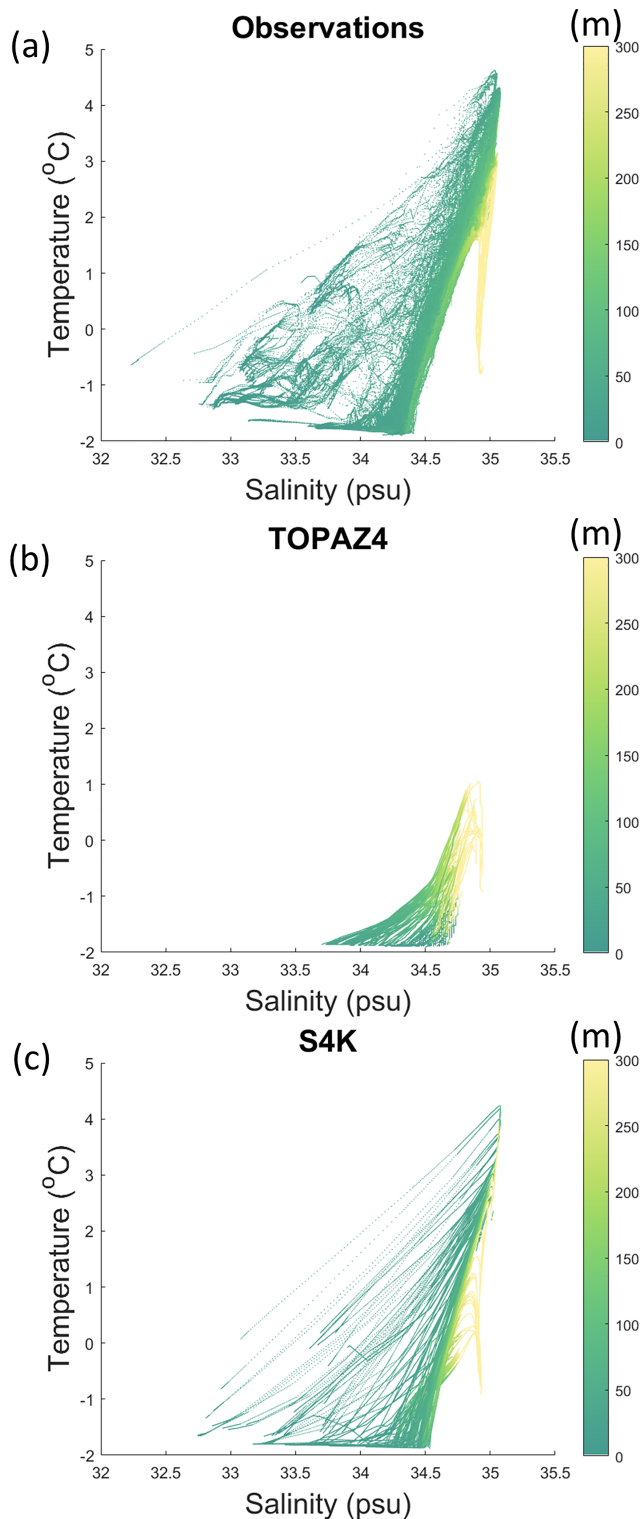


**Figure 7.** Temperature–salinity diagrams for observations collected during the N-ICE2015 expedition (Granskog et al., 2018). (a) TOPAZ4 and S4K models for the same periods and locations as the observations (b, c), respectively. The color scale represents depth in meters (see Fig. 1, Table 5 and text).

### 3.2.2 Sea ice results

Sea ice concentration and sea ice plus snow thickness from satellite products, TOPAZ4 and S4K show similar patterns (Figs. 8 and 9). In Figs. 8e–f and 9d, we plot S4K fields within a rectangle defined by a dashed line and “surrounded” by TOPAZ4 fields to evaluate the transition from TOPAZ4 forcing to the S4K fields. Boundary effects resulting from forcing S4K with TOPAZ4 sea ice data are not visible in the sea ice concentration plots (Fig. 8e and f) and they are quite smooth in the sea ice and snow thickness plots (Fig. 9d), with the exception of thinner ice along the northeast boundary in January 2015 (Fig. 9d). In some occasions, S4K predicts thin ice south eastwards of Greenland to a larger extent than observed in satellite data and protruding from the ice flowing along Greenland and out of the Fram Strait (Figs. 8f and 9d). This is neither visible in the satellite data nor in TOPAZ4 results (Figs. 8 and 9).

Sea ice and snow thickness results from S4K model are generally lower than those from satellite products and TOPAZ4 results for the overlapping areas (Fig. 9). However, sea ice and snow thickness frequency histograms based on EM31 data (Table 5) overlap more with S4K than to TOPAZ4 (Fig. 10a and b). A similar comparison based on HEM data shows similar trends (Fig. 10c and d). Despite the much smaller footprint of both the EM31 (3–5 m) and HEM data (50 m) (see Sect. 2.3.2) compared with the model resolution (12.5 km for TOPAZ4 and 4 km for S4K), the observed sea ice and snow thickness ranges are much larger than those predicted by both models. Regarding snow thickness based on Magnaprobe data, both models have a negative bias (Fig. 10e and f) and larger in absolute value than that for sea ice and snow thickness.

Here, we show only a limited number of results due to space constraints. However, monthly averaged map plots of sea ice concentration and sea ice plus snow thickness, from the satellite products listed in Table 5 and from TOPAZ4 and S4K for the period August 2014–July 2015) may be found at <https://doi.org/10.5281/zenodo.5800110> (Duarte, 2021).

## 4 Discussion

The implementation of time-varying boundaries both in the Barents-2.5 km and the S4K models, resulted in a generally smooth transition between the fields of TOPAZ4, providing the boundary conditions, and the fields of the former two models. The performance of the operational Barents-2.5 km improved significantly with the usage of time-varying sea ice boundaries. This upgraded performance was also a large contributor to the Barents-2.5 km operational forecasts being more widely adopted in downstream applications like drift models and vessel icing models and as support for a specific ship salvage operation near Svalbard. There is a large demand for more realistic operational forecasts to support

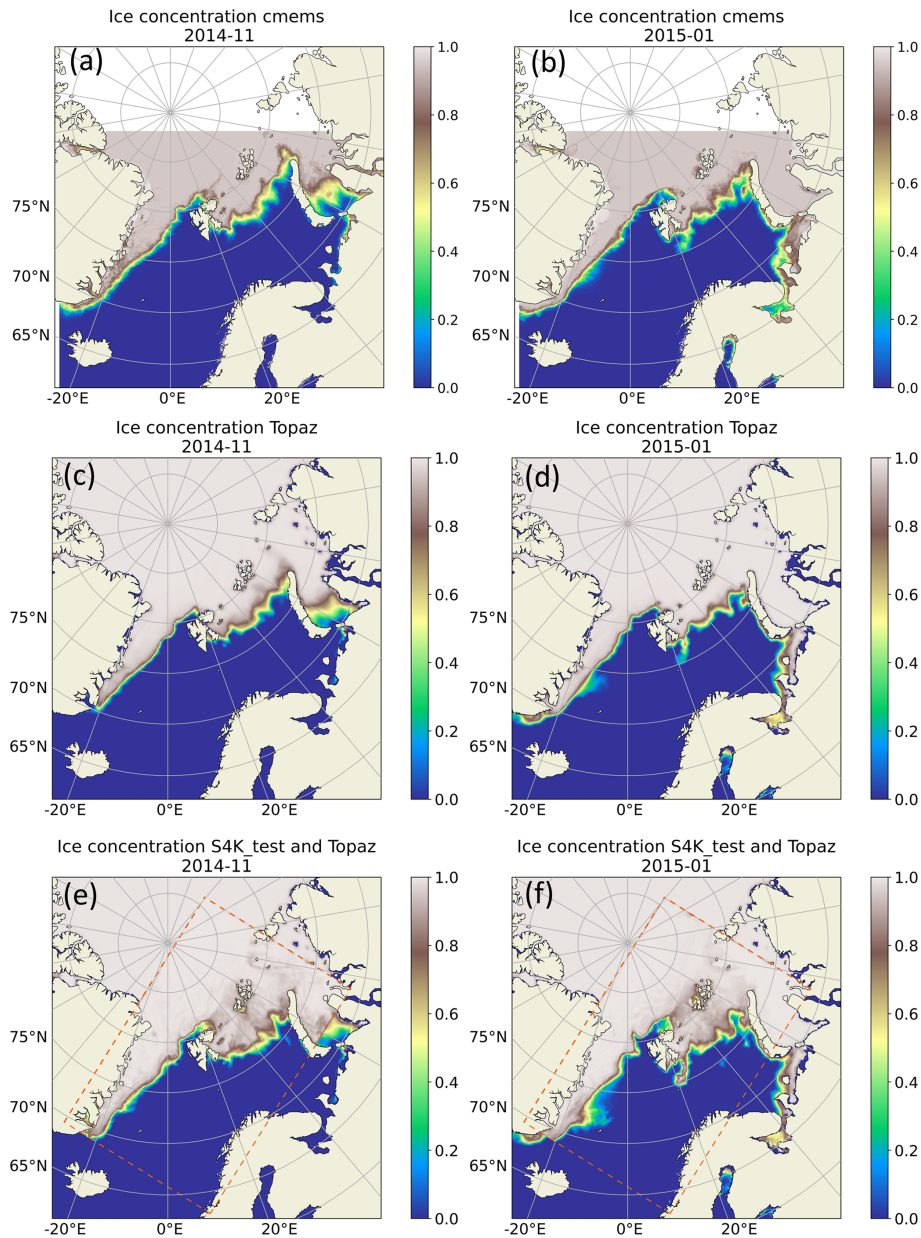


**Figure 8.** Dinessen and Hackett (2016) CMEMS (SEAICE\_ARC\_SEAICE\_L4\_NRT\_OBSERVATIONS\_011\_002) (a, b), TOPAZ (c, d) and S4K (e, f) results for monthly mean sea ice concentration fields for November 2014 (a, c, e) and January 2015 (b, d, f). S4K fields are inserted in the TOPAZ4 model domain in the rectangle defined by the dashed line included in panels (e) and (f) (see text).

search and rescue, oil spill and other similar scenarios in the Barents Sea. The implementation of a more realistic boundary treatment for sea ice is a central step to achieve a wider usage of the operational fields.

Notwithstanding these results, we still can see some “seams” between the TOPAZ4 fields and those of the other two models. For example, some ice and snow thickness “artifacts” are visible in the S4K model results, especially on the northeastern border of its domain (Fig. 10d). These “artifacts” may arise from drift differences inside the domain and

at the boundaries. Such artifacts were already noted in the Barents-2.5 km model (refer to Sect. 3.1.1). Another problem is the different horizontal spatial resolutions of TOPAZ4 (12.5 km) and the models described herein (2.5 and 4 km). Perhaps the more likely explanation is the mismatch between available TOPAZ4 sea ice fields and those required by CICE (refer to Sect. 2.2.2, model boundary data details). Recall from Sect. 2.2.2 that extensive assumptions had to be made in order to fit the limited TOPAZ4 data for all the boundary variables required by CICE. In fact, experiments (not shown)

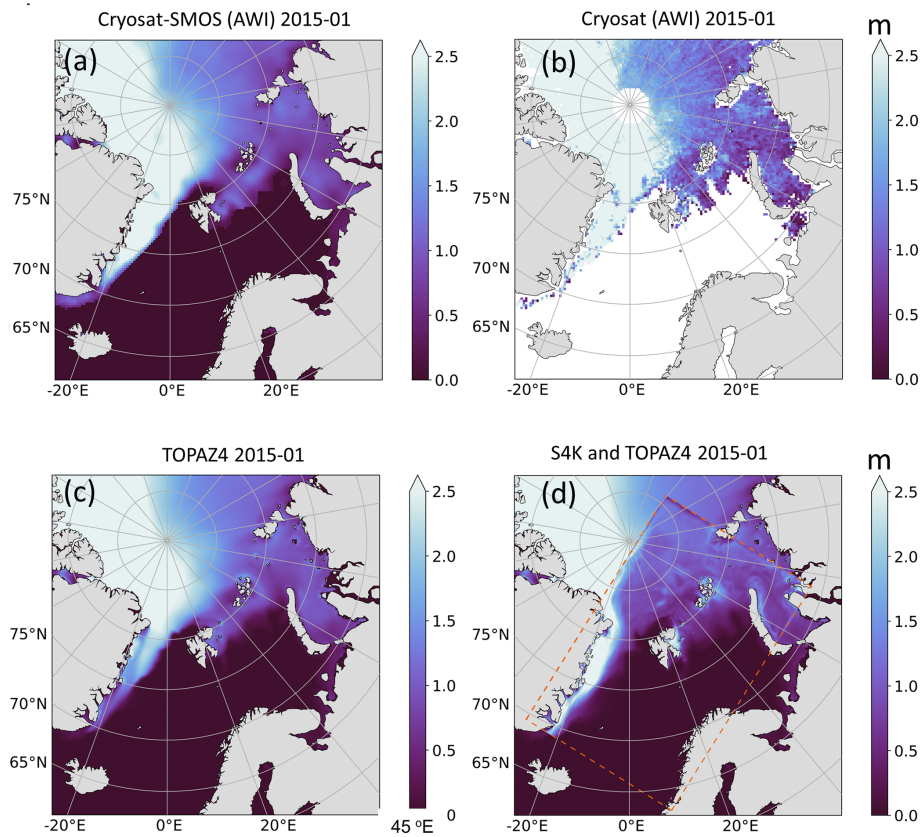


**Figure 9.** CryoSat2-SMOS (a), CryoSat-2 (b), TOPAZ4 (c) and S4K (d) monthly mean sea ice and snow thickness for January 2015. S4K fields are inserted in the TOPAZ4 model domain in the rectangle defined by the dashed line included in panel (d) (see text).

done with a higher-resolution model (500 m horizontal resolution) implemented with CICE, nested in the Barents-2.5 km model, and using exactly the same sea ice data of the larger model, did not show any seam but instead, a near-perfect transition between both domains. This shows the importance of coordinating the storage of adequate outputs from larger models with the “needs” of regional models. The ideal output from a larger model should include the variables listed in Table 2 (corresponding to the variables defined to store boundary values) and use the same sea ice thickness categories of the nested model and the same number of sea ice and snow layers.

In the tests carried out so far, we “relaxed” only the halo zone (more specifically, the grid cells surrounding the domain) and their neighbor cells to follow exactly the way CICE deals with boundary conditions. The default value in CICE for the thickness of this zone is one cell. In fact, this halo zone includes not only the domain boundaries but also the boundaries of all blocks of cells used in a parallel simulation. However, the boundary code affects only the cells surrounding the domain. A more complex treatment involving a broader relaxation zone with more than one cell thickness may be considered, but it is out of the scope of the present study.

The S4K model has a smaller ocean temperature and salinity bias than that of TOPAZ4, in the region north of Svalbard, where the N-ICE2015 expedition took place (Granskog et al., 2018). Observed biases are larger at the depth range where Atlantic Water and modified Atlantic Water are found (Meyer et al., 2017). There is a better fit between TOPAZ4 results and satellite data than those of S4K, which may partly result from the data assimilation process of the former. “Spurious” thin sea ice predicted by S4K southeastwards of Greenland (see Sect. 3.2.2 and Fig. 8f) results from the placement of the front between the inflowing Atlantic Water and the outflowing Polar Surface Water (e.g., Våge et al., 2018). In the S4K model, this front is not close enough to east Greenland on some occasions, allowing very cold surface water to spread towards Svalbard, with production of some thin sea ice.

As a final note, we emphasize here the compatibility of the changes described in this study with the most recent versions of the Los Alamos Sea Ice Model (CICE and ICEPACK), since the files changed and listed in Table 1 are similar to those of the most recent versions.

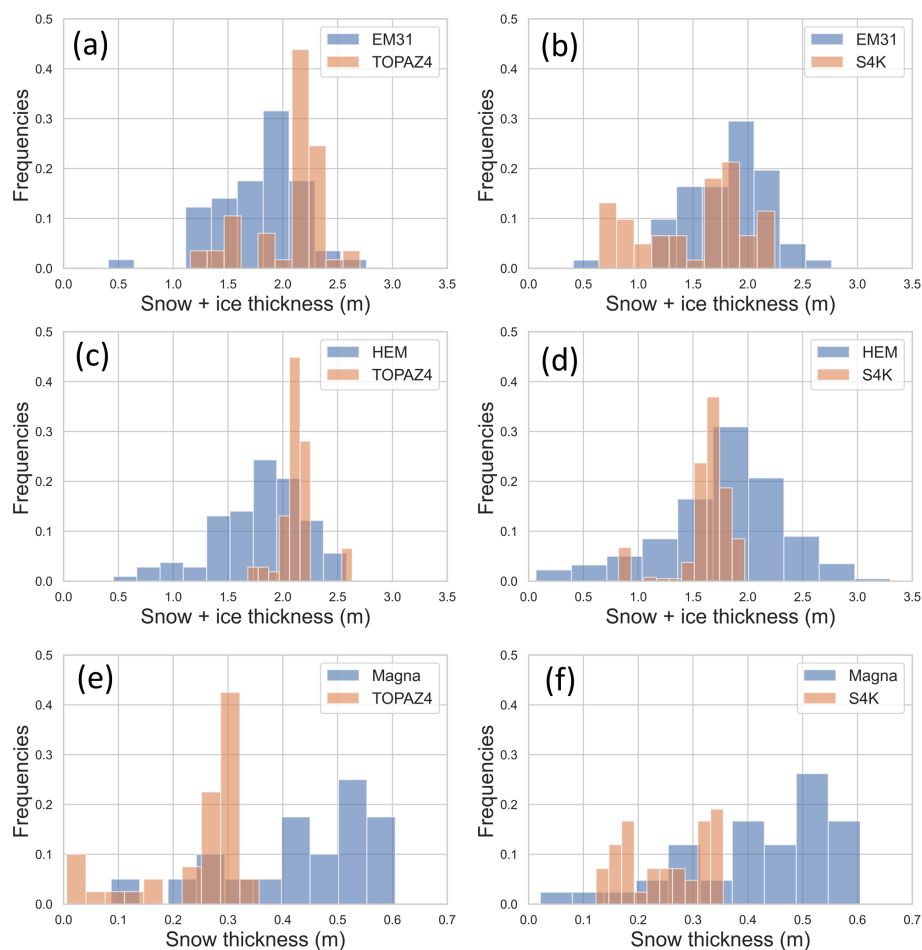


**Figure 10.** Observed (blue) and modeled (brown) frequency distributions of snow and ice thickness (a–d) and only snow thickness (e–f). Measurements were taken during the N-ICE2015 expedition with the instruments indicated at the top of the panels: EM31 (a, b) and HEM (c, d), for snow and ice thickness and Magnaprobe (e, f) for snow thickness. Observational data were averaged for TOPAZ4 (a, c, e) or S4K models cells located in the same areas, resulting in slightly different observed frequency distributions, given the different spatial resolution of the models (12.5 and 4 km, respectively). Model results, averaged for the same areas and days where measurements took place: (a, c, e) from TOPAZ4 and (b, d, f) from S4K (refer to Table 5 and text).

## 5 Conclusion

We implemented time-varying sea ice boundaries in the Los Alamos Sea Ice Model (CICE). This implementation was tested using two regional coupled ocean–sea ice models, both covering a large part of the Barents Sea and areas around Svalbard: the Barents-2.5 km, an operational forecast model, and the S4K, a model used for research purposes. Sea ice boundary conditions were obtained in both cases from TOPAZ4 – a well-tested and documented assimilative coupled ocean and sea ice model covering the Arctic and North Atlantic oceans. Obtained results show significant improvements in the performance of the Barents-2.5 km model after the implementation of the time-varying boundary conditions. The performance of the S4K model in terms of sea ice and snow thickness is comparable to that of the TOPAZ4 system. The implementation of time-varying boundary conditions de-

scribed in this study is similar regardless of the CICE versions used in different models. The main challenge remains the handling of data from larger models before its usage as boundary conditions for regional/local sea ice models, since mismatches between available model products from the former and specific requirements of the latter are expected, implying case-specific approaches and different assumptions. Ideally, model setups should be as similar as possible to allow a smoother transition from larger to smaller domains.

*Code availability.* The software code used in this study for the Barents-2.5 km model may be found at <https://doi.org/10.5281/zenodo.5067164> (Debernard et al., 2021).

The ocean modeling code is a ROMS branch. Code licensing may be found at [http://www.myroms.org/index.php?page=License\\_ROMS](http://www.myroms.org/index.php?page=License_ROMS) (last access: 17 May 2022).

The software code used in this study for the SA4 model may be found at <https://doi.org/10.5281/zenodo.5815093> (Duarte, 2022).

**Data availability.** Results from the Barents-2.5 km model may be found at <https://doi.org/10.5281/zenodo.4727865> (Brændshøi, 2021a) and <https://doi.org/10.5281/zenodo.4728069> (Brændshøi, 2021b) for the idealized and operational simulations, respectively, described in Sect. 2.4.1.

Graphical sea ice and snow results from the TOPAZ4 and S4K simulations may be found at <https://doi.org/10.5281/zenodo.5800110> (Duarte, 2021).

**Author contributions.** PD made the first version of software changes related to the implementation of time-varying boundaries in the CICE code and ran the simulations with the S4K model. JB, YG and NS implemented, tested, and adapted those changes in the Barents-2.5 km model and ran the simulations shown in the paper with this operational model. DS performed software development and implemented and tuned the S4K model. PB processed and helped analyze S4K model results. JA and AM contributed to the analysis of the S4K model results. AS provided the boundary conditions from TOPAZ4. KW prepared the AMSR2 sea ice concentration and its standard deviation and performed the data assimilation. JBD led and performed the implementation of the CICE–ROMS coupling in METROMS and contributed to discussions of the OBC implementation in Barents-2.5 km model. All authors contributed to the writing of the paper.

**Competing interests.** The contact author has declared that neither they nor their co-authors have any competing interests.

**Disclaimer.** Publisher’s note: Copernicus Publications remains neutral with regard to jurisdictional claims in published maps and institutional affiliations.

**Acknowledgements.** We acknowledge the usage of CryoSat-2 satellite products from the Alfred Wegener Institute (AWI), publicly available under a Creative Commons Attribution 4.0 International (CC BY 4.0) license, and the usage of CryoSat2-SMOS satellite products. We thank the US Department of Energy’s (DOE) Earth System Modeling Program for allowing the use of this version of the CICE model, which includes updated biogeochemistry parameterizations within a “column package” developed as part of the Accelerated Climate Model for Energy (ACME) project. Tuning and model validation work performed under the DOE Regional and Global Climate Modeling Program also contributed to these results.

**Financial support.** This work has been supported by the Fram Centre Arctic Ocean flagship project “Mesoscale physical and biogeo-

chemical modeling of the ocean and sea-ice in the Arctic Ocean” (project reference 66200), the Norwegian Metacenter for Computational Science application “NN9300K – Ecosystem modeling of the Arctic Ocean around Svalbard”, the Norwegian “Nansen Legacy” project (grant no. 276730), the European Union’s Horizon 2020 research and innovation program under grant agreement no. 869154 via project FACE-IT (The future of Arctic coastal ecosystems – Identifying transitions in fjord systems and adjacent coastal areas), the “Arktis 2030” program, and the project “Vrog havvarsling for arktisk miljøberedskap” funded by the Norwegian Ministry of Climate and Environment, as well as the European Union’s Horizon 2020 research and innovation program under grant agreement no. 101003826 via project CRiceS (Climate Relevant interactions and feedbacks: the key role of sea ice and Snow in the polar and global climate system). The production of the merged CryoSat2-SMOS sea ice thickness data was funded by the ESA project SMOS & CryoSat-2 Sea Ice Data Product Processing and Dissemination Service, and data from DATE to DATE were obtained from AWI.

**Review statement.** This paper was edited by Christopher Horvat and reviewed by two anonymous referees.

## References

- Beldring, S., Engeland, K., Roald, L. A., Sælthun, N. R., and Voksø, A.: Estimation of parameters in a distributed precipitation-runoff model for Norway, *Hydrol. Earth Syst. Sci.*, 7, 304–316, <https://doi.org/10.5194/hess-7-304-2003>, 2003.
- Brændshøi, J.: Model run with METROMS to evaluate open boundary conditions in CICE [idealized wind], Zenodo [data set], <https://doi.org/10.5281/zenodo.4727865>, 2021a.
- Brændshøi, J.: Model run with METROMS to evaluate open boundary conditions in CICE, Zenodo [data set], <https://doi.org/10.5281/zenodo.4728069>, 2021b.
- Debernard, J., Kristensen, N. M., Maartensson, S., Wang, K., Hedstrom, K., Brændshøi, J., and Szapiro, N.: metno/metroms: Version 0.4.1 (v0.4.1), Zenodo [code], <https://doi.org/10.5281/zenodo.5067164>, 2021.
- Dinessen, F. and Hackett, B.: Product user manual for regional high resolution sea ice charts Svalbard region SEAICE\_ARC\_SEAICE\_L4\_NRT\_OBSERVATIONS\_011\_002 (version 2.3), Copernicus, <https://www.yumpu.com/en/document/view/45590964/product-user-manual-for-regional-high-myoccean> (last access: 2 June 2022), 2016.
- Dodd, P., Meyer, A., Koenig, Z., Cooper, A., Smedsrud, L. H., Muilwijk, M., Rerolle, V., Kusse-Tiuz, N., Miguët, J., Onarheim, I., Davis, P., and Randelhoff, A.: N-ICE2015 ship-based conductivity-temperature-depth (CTD) data, Norwegian Polar Institute [data set], <https://doi.org/10.21334/npolar.2017.92262a9c>, 2016.
- Duarte, P.: Sea ice satellite and model data between October 2014 and December 2015 (v1.1), Zenodo [data set], <https://doi.org/10.5281/zenodo.5800110>, 2021.
- Duarte, P.: MCT, CICE and ROMS code used with for the S4K simulations (v1.1), Zenodo [code], <https://doi.org/10.5281/zenodo.5815093>, 2022.

- Egbert, G. D. and Erofeeva, S. Y.: Efficient inverse Modelling of barotropic ocean tides, *J. Atmos. Ocean. Tech.*, 19, 183–204, [https://doi.org/10.1175/1520-0426\(2002\)019<0183:Eimobo>2.0.Co;2](https://doi.org/10.1175/1520-0426(2002)019<0183:Eimobo>2.0.Co;2), 2002.
- Fritzner, S., Graverson, R., Christensen, K. H., Rostosky, P., and Wang, K.: Impact of assimilating sea ice concentration, sea ice thickness and snow depth in a coupled ocean–sea ice modelling system, *The Cryosphere*, 13, 491–509, <https://doi.org/10.5194/tc-13-491-2019>, 2019.
- Gerland, S., Winther, J. G., Orbaek, J. B., and Ivanov, B. V.: Physical properties, spectral reflectance and thickness development of first year fast ice in Kongsfjorden, Svalbard, *Polar Res.*, 18, 275–282, <https://doi.org/10.3402/polar.v18i2.6585>, 1999.
- Granskog, M. A., Fer, I., Rinke, A., and Steen, H.: Atmosphere–Ice–Ocean–Ecosystem Processes in a Thinner Arctic Sea Ice Regime: The Norwegian Young Sea ICE (N-ICE2015) Expedition, *J. Geophys. Res.-Oceans*, 123, 1586–1594, <https://doi.org/10.1002/2017jc013328>, 2018.
- Haas, C., Lobach, J., Hendricks, S., Rabenstein, L., and Pfaffling, P.: Helicopter-borne measurements of sea ice thickness, using a small and lightweight, digital em system, *J. Appl. Geophys.*, 67, 234–241, <https://doi.org/10.1016/j.jappgeo.2008.05.005>, 2009.
- Hattermann, T., Isachsen, P. E., von Appen, W. J., Albrechtsen, J., and Sundfjord, A.: Eddy-driven recirculation of Atlantic Water in Fram Strait, *Geophys. Res. Lett.*, 43, 3406–3414, <https://doi.org/10.1002/2016GL068323>, 2016.
- Hendricks, S. and Ricker, R.: Product User Guide & Algorithm Specification: AWI CryoSat-2 Sea Ice Thickness (version 2.3), <https://epic.awi.de/id/eprint/53331/> (last access: 17 May 2022), 2020.
- Hunke, E., Allard, R., Blain, P., Blockley, E., Feltham, D., Fichefet, T., Garric, G., Grumbine, R., Lemieux, J. F., Rasmussen, T., Ribergaard, M., Roberts, A., Schweiger, A., Tietsche, S., Tremblay, B., Vancoppenolle, M., and Zhang, J. L.: Should Sea-Ice Modeling Tools Designed for Climate Research Be Used for Short-Term Forecasting?, *Curr. Clim. Change Rep.*, 6, 121–136, <https://doi.org/10.1007/s40641-020-00162-y>, 2020.
- Hunke, E. C., Lipscomb, W. H., Turner, A. K., Jeffery, N., and Elliot, S.: CICE: the Los Alamos Sea Ice Model, Documentation and User's Manual Version 5.1, Los Alamos National Laboratory, USA, LA-CC-06-012, <http://www.ccpo.odu.edu/~klinck/Reprints/PDF/cicedoc2015.pdf> (last access: 2 June 2022), 2015.
- Jakobsson, M., Mayer, L., Coakley, B., Dowdeswell, J. A., Forbes, S., Fridman, B., Hodnesdal, H., Noormets, R., Pedersen, R., Rebesco, M., Schenke, H. W., Zarayskaya, Y., Accettella, D., Armstrong, A., Anderson, R. M., Bienhoff, P., Camerlenghi, A., Church, I., Edwards, M., Gardner, J. V., Hall, J. K., Hell, B., Hestvik, O., Kristoffersen, Y., Marcussen, C., Mohammad, R., Mosher, D., Nghiem, S. V., Pedrosa, M. T., Travaglini, P. G., and Weatherall, P.: The International Bathymetric Chart of the Arctic Ocean (IBCAO) Version 3.0, *Geophys. Res. Lett.*, 39, L12609, <https://doi.org/10.1029/2012gl052219>, 2012.
- Jeffery, N., Elliott, S., Hunke, E. C., Lipscomb, W. H., and Turner, A. K.: Biogeochemistry of CICE: The Los Alamos Sea Ice Model, Documentation and User's Manual. Zbgc\_colpkg modifications to Version 5, Los Alamos National Laboratory, Los Alamos, N. M., <https://doi.org/10.2172/1329842>, 2016.
- King, J., Gerland, S., Spreen, G., and Bratrein, M.: N-ICE2015 sea-ice thickness measurements from helicopter-borne electromagnetic induction sounding, Norwegian Polar Institute [data set], <https://doi.org/10.21334/npolar.2016.aa3a5232>, 2016.
- Mernild, S. H. and Liston, G. E.: Greenland Freshwater Runoff. Part II: Distribution and Trends, 1960–2010, *J. Climate*, 25, 6015–6035, <https://doi.org/10.1175/JCLI-D-11-00592.1>, 2012.
- Meyer, A., Fer, I., Sundfjord, A., Peterson, A. K., Smedsrud, L. H., Muilwijk, M., Randelhoff, A., Håvik, L., Koenig, Z., Onarheim, I., Davis, P., Miguët, J., and Kusse-Tiuz, N.: N-ICE2015 ocean microstructure profiles (MSS90L), Norwegian Polar Institute [data set], <https://doi.org/10.21334/npolar.2016.774bf6ab>, 2016.
- Meyer, A., Sundfjord, A., Fer, I., Provost, C., Robineau, N. V., Koenig, Z., Onarheim, I. H., Smedsrud, L. H., Duarte, P., Dodd, P. A., Graham, R. M., Schmidtko, S., and Kauko, H. M.: Winter to summer oceanographic observations in the Arctic Ocean north of Svalbard, *J. Geophys. Res.-Oceans*, 122, 6218–6237, <https://doi.org/10.1002/2016jc012391>, 2017.
- Müller, M., Batrak, Y., Kristiansen, J., Køltzow, M. A. Ø., Noer, G., and Korosov, A.: Characteristics of a Convective-Scale Weather Forecasting System for the European Arctic, *Mon. Weather Rev.*, 145, 4771–4787, <https://doi.org/10.1175/MWR-D-17-0194.1>, 2017.
- Naughten, K. A., Galton-Fenzi, B. K., Meissner, K. J., England, M. H., Brassington, G. B., Colberg, F., Hattermann, T., and Debernard, J. B.: Spurious sea ice formation caused by oscillatory ocean tracer advection schemes, *Ocean Model.*, 116, 108–117, <https://doi.org/10.1016/j.ocemod.2017.06.010>, 2017.
- Naughten, K. A., Meissner, K. J., Galton-Fenzi, B. K., England, M. H., Timmermann, R., Hellmer, H. H., Hattermann, T., and Debernard, J. B.: Intercomparison of Antarctic ice-shelf, ocean, and sea-ice interactions simulated by MetROMS-iceshelf and FESOM 1.4, *Geosci. Model Dev.*, 11, 1257–1292, <https://doi.org/10.5194/gmd-11-1257-2018>, 2018.
- Prakash, A., Zhou, Q., Hattermann, T., Bao, W., Graverson, R., and Kirchner, N.: A nested high-resolution unstructured grid 3-D ocean–sea ice–ice shelf setup for numerical investigations of the Petermann ice shelf and fjord, *MethodsX*, 9, 101668, <https://doi.org/10.1016/j.mex.2022.101668>, 2022.
- Rasmussen, T. A. S., Hoyer, J. L., Ghent, D., Bulgin, C. E., Dybkjaer, G., Ribergaard, M. H., Nielsen-Englyst, P., and Madsen, K. S.: Impact of Assimilation of Sea-Ice Surface Temperatures on a Coupled Ocean and Sea-Ice Model, *J. Geophys. Res.-Oceans*, 123, 2440–2460, <https://doi.org/10.1002/2017JC013481>, 2018.
- Ricker, R., Hendricks, S., Kaleschke, L., Tian-Kunze, X., King, J., and Haas, C.: A weekly Arctic sea-ice thickness data record from merged CryoSat-2 and SMOS satellite data, *The Cryosphere*, 11, 1607–1623, <https://doi.org/10.5194/tc-11-1607-2017>, 2017.
- Roberts, A., Craig, A., Maslowski, W., Osinski, R., DuVivier, A., Hughes, M., Nijssen, B., Cassano, J., and Brunke, M.: Simulating transient ice–ocean Ekman transport in the Regional Arctic System Model and Community Earth System Model, *Ann. Glaciol.*, 56, 211–228, <https://doi.org/10.3189/2015AoG69A760>, 2015.
- Rösel, A., Divine, D., King, J. A., Nicolaus, M., Spreen, G., Itkin, P., Polashenski, M., Liston, G. E., Ervik, Å., Espeseth, M., Gierisch, A., Haapala, J., Maaß, N., Oikkonen, A., Orsi, A., Shestov, A., Wang, C., Gerland, S., and Granskog, M. A.: N-ICE2015 total (snow and ice) thickness data from EM31, Norwegian Polar Institute [data set], <https://doi.org/10.21334/npolar.2016.70352512>, 2016a.

- Rösel, A., Polashenski, C. M., Liston, G. E., King, J. A., Nicolaus, M., Gallet, J.-C., Divine, D., Itkin, P., Spreen, G., Ervik, Å., Espeseth, M., Gierisch, A., Haapala, J., Maaß, N., Oikkonen, A., Orsi, A., Shestov, A., Wang, C., Gerland, S., Granskog, M. A.: N-ICE2015 snow depth data with Magnaprobe, Norwegian Polar Institute [data set], <https://doi.org/10.21334/npolar.2016.3d72756d>, 2016b.
- Rousset, C., Vancoppenolle, M., Madec, G., Fichefet, T., Flavoni, S., Barthélemy, A., Benshila, R., Chanut, J., Levy, C., Masson, S., and Vivier, F.: The Louvain-La-Neuve sea ice model LIM3.6: global and regional capabilities, *Geosci. Model Dev.*, 8, 2991–3005, <https://doi.org/10.5194/gmd-8-2991-2015>, 2015.
- Sakov, P., Counillon, F., Bertino, L., Lisæter, K. A., Oke, P. R., and Korabev, A.: TOPAZ4: an ocean-sea ice data assimilation system for the North Atlantic and Arctic, *Ocean Sci.*, 8, 633–656, <https://doi.org/10.5194/os-8-633-2012>, 2012.
- Smedsrud, L. H., Budgell, W. P., Jenkins, A. D., and Ådlandsvik, B.: Fine-scale sea-ice modelling of the Storfjorden polynya, *Ann. Glaciol.*, 44, 73–79, 2006.
- Smith, G. C., Liu, Y., Benkiran, M., Chikhar, K., Surcel Colan, D., Gauthier, A.-A., Testut, C.-E., Dupont, F., Lei, J., Roy, F., Lemieux, J.-F., and Davidson, F.: The Regional Ice Ocean Prediction System v2: a pan-Canadian ocean analysis system using an online tidal harmonic analysis, *Geosci. Model Dev.*, 14, 1445–1467, <https://doi.org/10.5194/gmd-14-1445-2021>, 2021.
- Spreen, G., L. Kaleschke, and Heygster, G.: Sea ice remote sensing using AMSR-E 89-GHz channels, *J. Geophys. Res.*, 113, C02S03, <https://doi.org/10.1029/2005JC003384>, 2008.
- Taylor, K. E.: Summarizing multiple aspects of model performance in a single diagram, *J. Geophys. Res.*, 106, 7183–7192, <https://doi.org/10.1029/2000JD900719>, 2001.
- Våge, K., Papritz, L., Havik, L., Spall, M. A., and Moore, G. W. K.: Ocean convection linked to the recent ice edge retreat along east Greenland, *Nat. Commun.*, 9, 1287, <https://doi.org/10.1038/S41467-018-03468-6>, 2018.
- Wang, K., Debernard, J., Sperrevik, A., Isachsen, P., and Lavergne, T.: A combined optimal interpolation and nudging scheme to assimilate OSISAF sea-ice concentration into ROMS, *Ann. Glaciol.*, 54, 8–12, <https://doi.org/10.3189/2013AoG62A138>, 2013.
- Wei, T., Yan, Q., Qi, W., Ding, M. H., and Wang, C. Y.: Projections of Arctic sea ice conditions and shipping routes in the twenty-first century using CMIP6 forcing scenarios, *Environ. Res. Lett.*, 15, 104079, <https://doi.org/10.1088/1748-9326/abb2c8>, 2020.
- Xie, J., Bertino, L., Counillon, F., Lisæter, K. A., and Sakov, P.: Quality assessment of the TOPAZ4 reanalysis in the Arctic over the period 1991–2013, *Ocean Sci.*, 13, 123–144, <https://doi.org/10.5194/os-13-123-2017>, 2017.